https://doi.org/10.5194/egusphere-2024-2885
Preprint. Discussion started: 16 October 2024

Duration of vegetation green-up response to snowmelt on the Tibetan Plateau

Jingwen Ni[1,2,3], Jin Chen[4], Yao Tang[1,2,3], Jingyi Xu[1,2,3,5], Jiahui Xu[1,2,3], Linxin Dong[1,2,3], Qingyu Gu[1,2,3], Bailang Yu[1,2,3], Jianping Wu[1,2,3], Yan Huang[1,2,3]

[1]Key Laboratory of Geographic Information Science, Ministry of Education, East China Normal University, Shanghai 200241, China
[2]School of Geographic Sciences, East China Normal University, Shanghai 200241, China
[3]Key Laboratory of Spatial-temporal Big Data Analysis and Application of Natural Resources in Megacities, Ministry of Natural Resources, Shanghai, 200241, China
[4]State Key Laboratory of Earth Surface Processes and Resource Ecology, Beijing Normal University, Beijing 100875, China
[5]Zhejiang Tiantong Forest Ecosystem National Observation and Research Station, School of Ecological and Environmental Sciences, East China Normal University, Shanghai 200241, China

Correspondence to: Yan Huang (yhuang@geo.ecnu.edu.cn)

Abstract. The Tibetan Plateau (TP) is characterized by abundant snow and heightened sensitivity to climate change. Although the impact of snowmelt on vegetation green-up is well recognized, the duration of the vegetation response to snowmelt on the TP remains unclear. This study calculates the time differences between the green-up date and the start of snowmelt from 2001 to 2018 on the TP, denoted as ΔT. Exploratory spatial data analysis and Mann Kendall test were then applied to investigate the spatiotemporal distribution feature of ΔT. Subsequently, heatmaps, box plots, partial correlation, and multiple linear regression analyses were employed to examine the impact of spring mean temperature, spring total rainfall, and daily snowmelt on ΔT. The results reveal that the mean ΔT across the TP was 36.7 days, with a spatially clustered distribution: low-low clusters in the Hengduan Mountains and high-high clusters in the Bayankara and Himalayas Mountains. Additionally, ΔT shortened with increasing spring mean temperature, spring total rainfall, and daily snowmelt, which can explain 15.7%, 16.1%, and 25.8% of ΔT variation, respectively. In arid areas and regions with low vegetation, daily snowmelt was the dominant factor of ΔT for 74% and 66% of the regions, respectively. Conversely, spring mean temperature was the predominant factor for 65% and 59% of humid areas and regions with high vegetation. Our findings enhance the understanding of vegetation responses to snowmelt and provide a scientific basis for further research on the stability of alpine ecosystems and the impacts of climate change on the TP.

1 Introduction

The Tibetan Plateau (TP) is the largest plateau in China and the highest in the world. It serves as the source for many major Asian rivers, providing water resources to approximately 1.6 billion people (Bibi et al., 2018). Additionally, the TP plays a critical role in maintaining global biodiversity and ecological security (Piao et al., 2019). Over the past 50 years, climate change has caused the mean temperature of the TP to rise at twice the global rate (Yang et al., 2019; Zhang et al., 2018a).

https://doi.org/10.5194/egusphere-2024-2885
Preprint. Discussion started: 16 October 2024

Plant phenology, which reflects climatic patterns and influences climate through biological and biochemical processes, is a key aspect of this change (Piao et al., 2019; Zhang et al., 2022b). Specifically, the green-up date (T_{GU}), marking the onset of vegetation growth under favorable climatic conditions (Zhang et al., 2003), is a vital indicator for studying climate change (Shen et al., 2015). Therefore, understanding the changes and mechanisms affecting T_{GU} is essential for assessing the impact of climate change on the TP and its ecological stability.

Previous studies on the climatic factors influencing T_{GU} have primarily focused on temperature and precipitation, as these are the two most significant determinants of T_{GU} (Zhang et al., 2022a). However, the impact of snow on T_{GU} should not be ignored (Wang et al., 2018a). Snow affects vegetation mainly through its influence on soil temperature, soil moisture, soil nutrients, and photosynthetically active radiation. Specifically, snow cover can mitigate the exchange of soil heat and moisture with the atmosphere (Zhu et al., 2019a), leading to smaller annual variations in soil temperature compared to air temperature (Zhang et al., 2018b), and thus providing a more favorable overwintering environment for vegetation (Zhu et al., 2019a). Furthermore, snowmelt increases soil moisture, promoting vegetation growth (Peng et al., 2010; Potter, 2020). Changes in soil temperature and moisture due to snow cover can also influence microbial activity, which in turn affects the availability of nutrients for vegetation (Ren et al., 2020; Wang et al., 2015). Nevertheless, the high albedo of snow reflects much of the solar radiation that is essential for photosynthesis (Rixen et al., 2022; Yang et al., 2022). Consequently, changes in snow cover invariably influence transitions in T_{GU}.

The TP has abundant snow cover. Snow phenology serves as a crucial indicator of changes in snow cover. Several studies have analyzed the impact of snow phenology on T_{GU} in the TP. Key aspects of snow phenology related to T_{GU} include the snow cover end date (SCED), snow cover duration (SCD), and the start of snowmelt (T_{SOM}). SCED typically exhibits a significant positive correlation with T_{GU}, with each 1-day advancement in SCED leading to a 0.56 days earlier T_{GU} (Potter, 2020; Wu et al., 2023). The effect of SCD on T_{GU} is more complex and varies by region; for instance, a longer SCD delays T_{GU} in the western TP, whereas an extended autumn SCD advances T_{GU} in the eastern TP (Huang et al., 2019; Xiong et al., 2019). Notably, T_{GU} is most sensitive to T_{SOM} among the various metrics of snow cover phenology on the TP (Xu et al., 2022a). Wang et al. (2015) found that 39.9% of meadows and 36.7% of steppes on the TP demonstrated a significant correlation between T_{GU} and T_{SOM}. Additionally, Wang et al. (2018a) reported positive Pearson correlation coefficients between T_{SOM} and T_{GU} for most regions of the TP, with exceptions in warmer and drier areas. Despite these findings, the duration and driving factors of vegetation response to the onset of snowmelt remain unclear.

In this study, the time difference between T_{GU} and T_{SOM}, denoted as ΔT, was used to represent the duration of the vegetation's green-up response to snowmelt. We firstly employed a daily snow depth dataset with a resolution of 0.05° to identify T_{SOM} and subsequently calculated ΔT for the TP from 2001 to 2018. Exploratory spatial data analysis and the Mann-Kendall test were employed to examine the spatiotemporal variation of ΔT. To quantify the influence of temperature, precipitation, and snowmelt on ΔT, we applied partial correlation analysis and multiple linear regression. Additionally, we evaluated the quality of ΔT and discussed the response mechanism of vegetation to snowmelt.

https://doi.org/10.5194/egusphere-2024-2885
Preprint. Discussion started: 16 October 2024

2 Materials and Methods

2.1 Study area

The TP, located between 25.99°N and 39.82°N and 73.46°E and 104.67°E, has an average elevation exceeding 4000 m (Fig. 1). The TP is characterized by distinct climatic patterns, including intense solar radiation and significant diurnal temperature variations. Winter temperatures range from −15 to −2 ℃, while summer temperatures average between 8 and18 ℃. Annual precipitation is approximately 400 mm, with the region transitioning from humid in the southeast to sub-humid, semiarid, and arid conditions in the northwest (Diao et al., 2021).

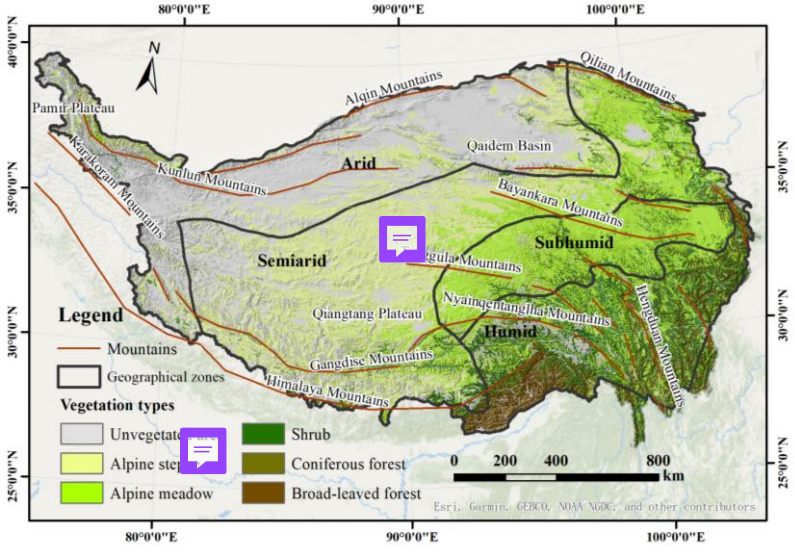

Figure 1: Map of the study area with vegetation types, distribution of mountains and geographical zones (based map from ESRI)

Due to substantial topographic uplift and its extensive spatial extent, the TP exhibits a diverse range of climate types and ecosystems. Predominant vegetation types include alpine meadows and alpine steppes, which are widespread across the central regions. The southeastern areas are primarily covered by forests and shrubs, while the western and northern regions are largely barren or desertified due to the terrain and climatic conditions (Zhao et al., 2011).

Snow cover on the TP shows clear spatial and seasonal variability. Except for the Himalayan Mountains, the Pamir Plateau, and the eastern sector of the Tanggula Mountains, which have perennial snow cover, other areas experience seasonal snow cover. Snow accumulation generally begins in September, persists from October to late November, and peaks from December to February. The mean snow cover fraction across the TP is 36.6% (Zou et al., 2022).

https://doi.org/10.5194/egusphere-2024-2885
Preprint. Discussion started: 16 October 2024

2.2 Data sources

2.2.1 Green-up date dataset

Remote sensing-based vegetation indices (VIs) are commonly used to identify the T_{GU}. However, different VIs and extraction methods can introduce uncertainties into the results (Shen et al., 2014). Xu et al. (2022b) compared six different vegetation indices and four extraction methods, finding that the Normalized Difference Greenness Index (NDGI) combined with the Maximum Curvature Change Rate method (CCRmax) yielded the highest identification accuracy (r = 0.62, RMSE = 11 days, $p < 0.01$) on the TP. Therefore, we utilized these data as T_{GU} for our study. The dataset, spanning from 2001 to 2018, had a spatial resolution of 500 m and was measured in Day of Year (DOY). To ensure consistent data resolution, we applied bilinear interpolation to reproject the dataset to a resolution of 0.05°.

2.2.2 Snow depth and snowmelt products

Daily snow depth data from 2001 to 2018 were used to identify the T_{SOM}. This dataset is accessible through the National Tibetan Plateau Data Center (https://data.tpdc.ac.cn/) and has a spatial resolution of 0.05°. Produced by Yan et al. (2022), it is based on a long-term series of daily snow depth data in China (1979–2023) (http://poles.tpdc.ac.cn/en/) and snow cover probability data derived from the Moderate Resolution Imaging Spectroradiometer (MODIS). Yan et al. (2022) employed a spatial-temporal downscaling method to improve spatial resolution from 0.25° to 0.05°, achieving greater accuracy compared to the original dataset (RMSE = 0.61 cm).

Snowmelt data for the period between 2001 and 2018 were sourced from ERA5-Land, provided by the Climate Data Store (https://cds.climate.copernicus.eu/cdsapp#!/home). This dataset integrates physical models with global reanalysis observations and has a spatial resolution of 0.1° and a temporal resolution of one hour. The snowmelt variable quantifies the total amount of water (m) produced by snow melting within snow-covered areas. The data were reprojected to a 0.05° resolution using bilinear interpolation, and the time resolution was adjusted to daily values through summation.

2.2.3 Meteorological dataset

Daily average air temperature and precipitation data from 2001 to 2018 were used to investigate the impact of meteorological factors on ΔT. These data were obtained from the China Meteorological Forcing Dataset (CMFD), provided by the National Tibetan Plateau Scientific Data Centre (https://data.tpdc.ac.cn/). The CMFD integrates remote sensing data with field observations, and due to its use of numerous actual observation sites, it offers higher accuracy compared to the Global Land Data Assimilation System (GLDAS) and ERA5-Land (He et al., 2020; Li et al., 2022). The CMFD dataset has a spatial resolution of 0.1° and a temporal resolution of 3 h, with units of K for temperature and mm h^{-1} for precipitation. To match our analysis requirements, we reprojected the dataset to a 0.05° resolution using bilinear interpolation and adjusted the temporal resolution to daily values by summing (for precipitation) and averaging (for air temperature).

https://doi.org/10.5194/egusphere-2024-2885
Preprint. Discussion started: 16 October 2024

2.2.4 Land cover type

The land cover type map of the TP (2010), which provided vegetation type information for this study, was sourced from the Science Data Bank (https://www.scidb.cn/en). This map was classified using the support vector machine method based on MODIS images, achieving a classification accuracy of 93% with a spatial resolution of 500 m. The map delineates ten land cover types on the TP: alpine desert, alpine steppe, alpine meadow, bare land/desert, arable land, shrub, coniferous forest, broad-leaved forest, permanent snow/glacier, and lake. Prior to use, the dataset was reprojected to a resolution of 0.05°.

2.3 Method

2.3.1 Subsubsection (as Heading 3) Calculation of ΔT

The time differences between T_{GU} and T_{SOM} (ΔT) can be calculated using the following equation:

$$\Delta T = T_{GU} - T_{SOM} \quad (1)$$

where T_{GU} and T_{SOM} are the green-up date and start of snowmelt, respectively, in DOY.

The T_{GU} dataset was provided by Xu et al. (2022b). They used the MODIS surface reflectance product MOD09A1 to calculate the vegetation index NDGI, which integrates red (band 1), near-infrared (band 2), and green (band 4) reflectances. The NDGI time series was then fitted with a four-parameter logistic function, and the curvature change rate (CCR) of the logistic function was calculated. T_{GU} was defined as the date on which the CCR reached its first local maximum.

T_{SOM} was identified from snow depth measurements. A snowfall event typically involves two stages: snow accumulation and snowmelt (Fontrodona-Bach et al., 2023), which are characterized by changes in snow depth. The maximum snow depth marks the transition between these two stages (Zheng et al., 2022) (see the orange point in Fig. 2). To determine T_{SOM}, the snow depth time series was first smoothed using Sacitzky-Golay filtering with a 5-day window to minimize the influence of outliers (as indicated by the orange line in Fig. 2). The date of the maximum snow depth in spring was then identified as T_{SOM}. Given that multiple snow accumulation and melting events may occur throughout the snow year on the TP (Lei et al., 2023), two criteria were established. First, the snow depth time series was analyzed starting from DOY 61 (March 1), as snowmelt before spring has minimal impact on vegetation dormancy and snowmelt on the TP typically begins in March (Dong et al., 2024). Second, the snowfall event with the longest duration of snow cover was considered the most significant. Thus, the number of consecutive snow cover days was compared to determine the turning point. According to Stanislaw et al. (2023), a snow cover day is defined as a day when the snow depth exceeds 1 cm. As illustrated in Fig. 2, Snow depth was above 1 cm from DOY 61 to DOY 107, making the duration of the first snowfall event 47 days. In contrast, the durations of the second and third events were 3 days and 6 days, respectively. The first snow accumulation and melting process was the longest; thus, the turning point on DOY 96 was designated as T_{SOM}.

https://doi.org/10.5194/egusphere-2024-2885
Preprint. Discussion started: 16 October 2024

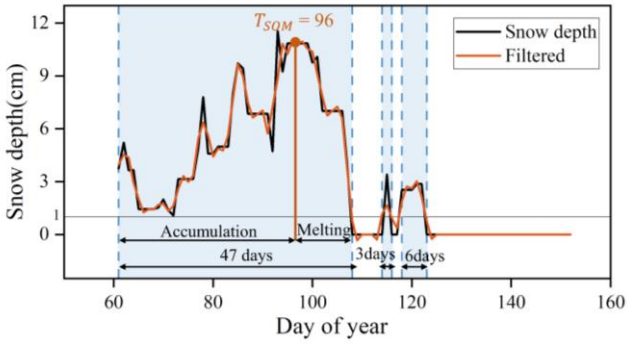

Figure 2. Diagram showing identification of start of snowmelt (T_{SOM}).

2.3.2 Exploratory Spatial Data Analysis

Classical statistical analysis models assume sample independence, which limits their ability to reveal correlations between the geographical locations of spatial data. Exploratory Spatial Data Analysis (ESDA) offers an enhancement over traditional methods by examining spatial discrepancies and autocorrelation in spatial datasets. Two commonly used indicators in ESDA are the global and local Moran's I. In this study, these indices are applied to analyze the spatial distribution of ΔT. The global Moran's I (I) measures the overall similarity of ΔT between a region and its neighboring regions, as detailed in Equation 2. The local Moran's I (I_i) assesses the degree of clustering or spatial autocorrelation of ΔT within a specific region i relative to its neighbors, as calculated using Equation 3.

$$I = \frac{n\sum_{i=1}^{n}\sum_{j=1}^{n} w_{ij}\,(x_i-\overline{x})(x_j-\overline{x})}{\sum_{i=1}^{n}\sum_{j=1}^{n} w_{ij}\sum_{i=1}^{n}(x_i-\overline{x})^2} \quad (2)$$

$$I_i = \frac{n(x_i-\overline{x})\sum_{j=1}^{n} w_{ij}\,(x_j-\overline{x})}{\sum_{i=1}^{n}(x_i-\overline{x})^2} \quad (3)$$

where x_i, x_j represent ΔT for region i and j, $\overline{x}$ is the mean value of ΔT, w_{ij} is the spatial weight between region i and region j, and n is the total number of regions.

Moran's I ranges from −1 to 1. A positive value indicates significant spatial autocorrelation, suggesting a tendency for spatial clustering. Conversely, a negative value signifies significant spatial autocorrelation, indicating a tendency for spatial dispersion. If the value is close to zero, the data is considered to be randomly distributed. The significance of spatial autocorrelation can be assessed using the p-value of the standardized Z-statistic (Equation 4).

$$Z = \frac{I - E(I)}{\sqrt{Var(I)}} \quad (4)$$

where I denotes the Moran's index, $E(I)$ represents the expectation value of I, and $Var(I)$ is the variance of I. A significance level of $p < 0.01$ is used to determine statistical significance.

https://doi.org/10.5194/egusphere-2024-2885
Preprint. Discussion started: 16 October 2024

2.3.3 Mann-Kendall Test

The Mann-Kendall test was used to investigate the temporal trend of ΔT from 2001 to 2018 for each pixel. Unlike traditional regression or trend fitting methods, this test does not require the samples to adhere to a specific distribution. Additionally, the Mann-Kendall test is robust to outliers, thereby minimizing disturbances (Howell et al., 2012).

First, the statistic S must be calculated, as shown in Equation 5. This statistic represents the sum of the indicator functions that compare the differences between years: if the latter year has a higher value than the former, the function returns 1; if it has a lower value, it returns −1; Otherwise, it returns 0 (Semmens and Ramage, 2013). The standardized statistic (Z_c) is then calculated using Equation 6.

$$S = \sum_{i=1}^{n-1} \sum_{j=i+1}^{n} sgn(x_j - x_i) \tag{5}$$

$$Z_c = \begin{cases} \dfrac{S+1}{\sqrt{Var(S)}}, & S < 0 \\ 0, & S = 0 \\ \dfrac{S-1}{\sqrt{Var(S)}}, & S > 0 \end{cases} \tag{6}$$

where n is the length of the time series $x_1, \dots x_i, x_j, \dots x_n$, $Var(S)$ is the variance of the statistic, and Z_c is used for trend testing. If $|Z_c| > Z_{1-\alpha/2}$, a significant temporal trend is present. Here, $Z_{1-\alpha/2}$ represents the standard normal variance, and α signifies the significance level. In this study, the significance levels were set at three thresholds: $\alpha = 0.01, \alpha = 0.05, \alpha = 0.1$.

If the time series exhibits a significant temporal trend, the trend in ΔT can be assessed using the parameter β (Equation 7).

$$\beta = Median\left(\frac{x_i - x_j}{i - j}\right) \tag{7}$$

where x_i, x_j are ΔT of year i and j, respectively. The median function is denoted by $Median$, and β indicates the degree of trend: an upward trend if $\beta > 0$ and a decline if $\beta < 0$.

2.3.4 The influence of meteorological and snow factors on ΔT

Spring temperature and precipitation exerted a profound influence on T_{GU}. Generally, temperature controls heat conditions, while precipitation provides the necessary water for vegetation (Shen et al., 2022). Recent studies have highlighted the varying responses of vegetation to snow phenology across different moisture and heat zones (Guan et al., 2022; Liu et al., 2023). Specifically, as temperature increased, the correlation between SCED and T_{GU} initially decreased below 0°C but then increased above 0°C (Wu et al., 2023). Increased humidity from precipitation strengthened the positive correlation between T_{SOM} and T_{GU}, whereas in high temperature areas, a strong negative correlation prevailed (Xu et al., 2022a). Besides temperature and precipitation, snowmelt significantly altered environmental conditions conducive to vegetation growth,

https://doi.org/10.5194/egusphere-2024-2885
Preprint. Discussion started: 16 October 2024

suggesting that the magnitude of snowmelt from T_{SOM} to T_{GU} may also influence ΔT (An et al., 2022; Rixen et al., 2022). Therefore, we selected the daily mean temperature of spring (T_{spring}), the total spring rainfall (P_{spring}), and the daily mean snowmelt from T_{SOM} to T_{GU} (S_{StoG}) as the influencing factors of ΔT.

The partial correlation coefficient between each variable and ΔT was computed to quantify the relationship. Next, a multiple linear regression model was established for each pixel (Equation 8).

$$\Delta T = aT_{spring} + bP_{spring} + cS_{StoG} + d \quad (8)$$

where a、b、c are the fitting coefficients used to determine the contribution of T_{spring}, P_{spring} and S_{StoG} to ΔT, respectively, while d represents a constant term. By comparing the fitting coefficients, the factor with the largest coefficient was deemed dominant.

It is important to note that all variables were standardized by Z-scores before being input into the model to eliminate dimensional differences. Additionally, since the models are based on the pixel scale, only regions with more than 6 years of ΔT were considered valid samples. The significance level was set at $p < 0.1$.

3 Result

3.1 Spatial and temporal distribution characteristics of ΔT

Figure 3 shows the spatial pattern of the multiyear mean T_{SOM} and T_{GU} data from 2001 to 2018. The Qaidam Basin and southern Qiangtang Plateau, which rarely experience snowfall (Xu et al., 2024), present challenges for snowmelt detection. In the northern TP, where vegetation is sparse, and in the southeastern TP, where seasonal vegetation changes are minimal, T_{GU} was not observed. Generally, T_{SOM} occurred between DOY 70 to 100 (10 March to 9 April) for 80.1% of the TP, with an average DOY of 86.1. The latest T_{SOM} (>DOY 105) was found in the Kunlun and Nyainqentanglha Mountains, while the earliest T_{SOM} occurred in the Hengduan and Minshan Mountains, with an averaged DOY of 76.8. In contrast, T_{GU} appeared later and was more concentrated, ranging from DOY 110 to 140 (19 April to 19 May) for 77.6% of the TP, showing a clear progress from west to east.

https://doi.org/10.5194/egusphere-2024-2885
Preprint. Discussion started: 16 October 2024

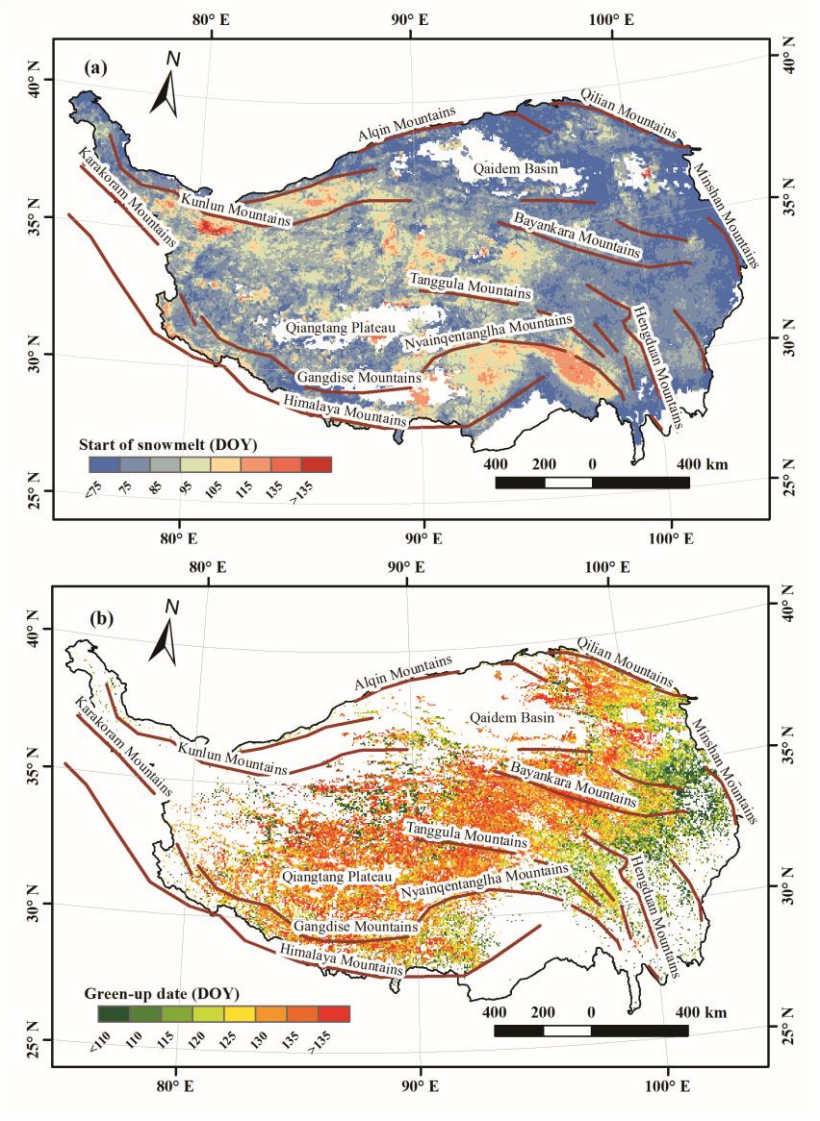

Figure 3: Spatial distribution of multiyear averaged (a)T_{SOM} and (b)T_{GU} from 2001 to 2018 on the Tibetan Plateau.

ΔT was calculated using Equation 1 for regions where both T_{SOM} and T_{GU} were non-null (Fig. 4). A positive ΔT indicates that T_{SOM} preceded T_{GU}, and vice versa. The average ΔT over the TP from 2001 to 2018 was 36.7 days, with positive values observed over 90% of the TP. The proportion of ΔT ranging from 40 to 60 days was the highest, accounting for 34.3% on average. Spatially, ΔT increases from approximately 27.8 days in the south to 39.7 days in the north of the southeast TP, with larger values (around 47.3 days) observed in the Bayankara, Gangdise, and Himalayas Mountains. Negative ΔT was mainly found in the central TP and some areas of the Qilian Mountains, averaging −25.9 days.

https://doi.org/10.5194/egusphere-2024-2885
Preprint. Discussion started: 16 October 2024

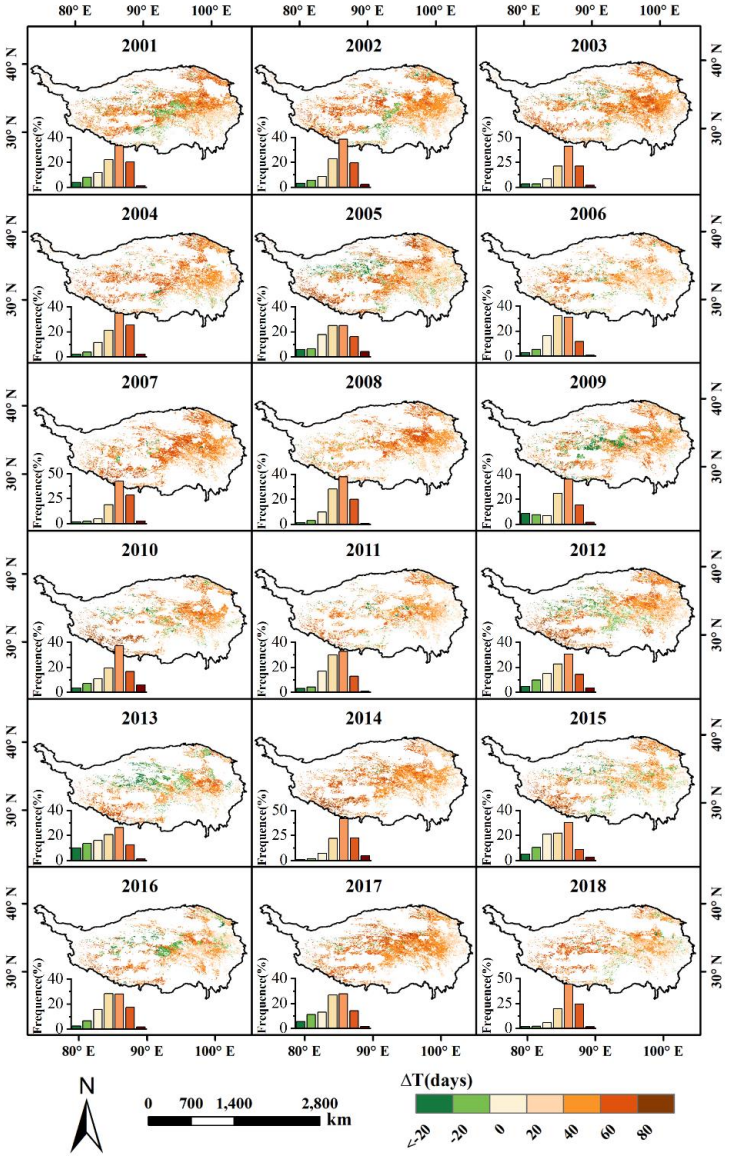

Figure 4: Spatial and frequency distribution histograms of ΔT on the Tibetan Plateau from 2001–2018.

The global and local Moran's I were calculated (Fig. 5), to gain more about spatial distribution characteristics of ΔT. The global Moran's I of ΔT over the TP from 2001–2018 was significant at the 0.01 level. Despite some annual fluctuations, the global Moran's I index consistently remained above zero and showed a gradual decrease from approximately 0.3 to 0.2 (left-bottom values in each subgraph of Fig. 5). This indicates that ΔT demonstrates spatial clustering with a slight reduction in its concentration. The local Moran's I index revealed that about 58.7% of the regions exhibited significant spatial autocorrelation. The pale blue regions in Fig. 5 represent low-value clustering, comprising 21.1% of the area, while the pink regions, accounting for 27.5%, indicate high-value clustering, meaning ΔT was generally longer in these areas. Red and blue

https://doi.org/10.5194/egusphere-2024-2885
Preprint. Discussion started: 16 October 2024

230 areas, representing high (low) values surrounded by low (high) values, accounted for 5.7 and 4.4%, respectively. The spatial distribution of ΔT clustering was relatively stable from 2001 to 2018, with low values predominatly concentrated in the Hengduan Mountains and high values primarily clustered around the Bayankara and Himalaya Mountains.

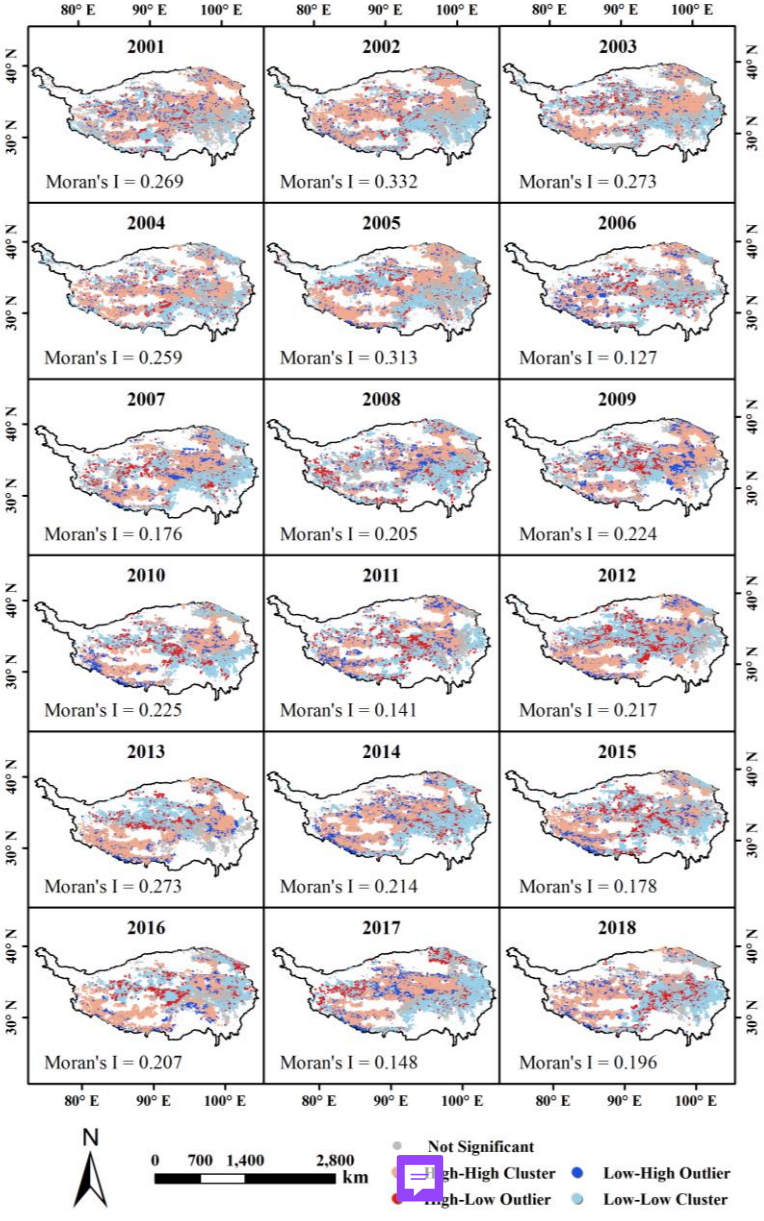

Figure 5: Global and local Moran's I values of ΔT on the Tibetan Plateau from 2001–2018.

235 Regarding the temporal trend of ΔT, Fig. 6 shows the interannual variation from 2001–2018, along with its significance indicated in the bottom-left corner. Only 6.2% of the study area, predominantly in the eastern TP, exhibits a

https://doi.org/10.5194/egusphere-2024-2885
Preprint. Discussion started: 16 October 2024

significant trend. Of these regions, approximately 86.6% show a declining trajectory, suggesting that vegetation in these areas responded more rapidly to snowmelt. However, for most regions, no discernible trend was observed over time, likely because the warming hiatus since the 2000s has not led to noticeable advancements in T_{SOM} and T_{GU} (Piao et al., 2019; Wang et al., 2019).

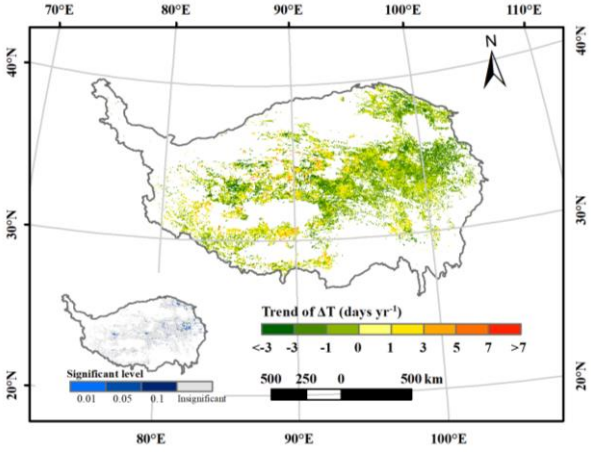

Figure 6: Interannual variation trend and significant levels of ΔT on the Tibetan Plateau from 2001–2018.

3.2 Influence of air temperature, precipitation, and snowmelt on ΔT

As observed in section 3.1, ΔT is positive in most regions. Furthermore, snowmelt only significantly impact vegetation when T_{SOM} precedes T_{GU}. Consequently, subsequent analyses will focus exclusively on areas where ΔT is positive.

Figure 7a illustrates the mean value of ΔT under varying spring meteorological conditions. Within each column, T_{spring} remains constant, while each row represents a fixed P_{spring}. ΔT exhibits a distinct stepwise decline from cold-arid to warm-humid regions, decreasing from approximately 50 to 30 days. Along the X-axis (with consistent moisture conditions), ΔT decreases as spring temperature rise. Near the freezing point (272–273 K), ΔT advances significantly by about three days. However, in regions below 273 K, ΔT fluctuates with temperature. In cold-humid areas, ΔT is prone to outliers and lacks a clear pattern due to the small sample size. Along the Y-axis (with constant thermal conditions), ΔT diminished with increasing rainfall, except in regions with temperatures between 264–267 K. For every additional 10 mm of rainfall, ΔT decreases by 0.1–5 days. Additionally, higher spring temperature amplify the reduction in ΔT with increased precipitation.

Fig. 7b reveals a strong negative correlation between ΔT and S_{StoG} when S_{StoG} exceeds 6 mm day^{-1}. An increase of 1 mm in S_{StoG} corresponds to an approximate decrease of 0.615 days in ΔT. The dispersion within each snowmelt category remains relatively constant, with a standard deviation of about 16.8 days.

https://doi.org/10.5194/egusphere-2024-2885
Preprint. Discussion started: 16 October 2024

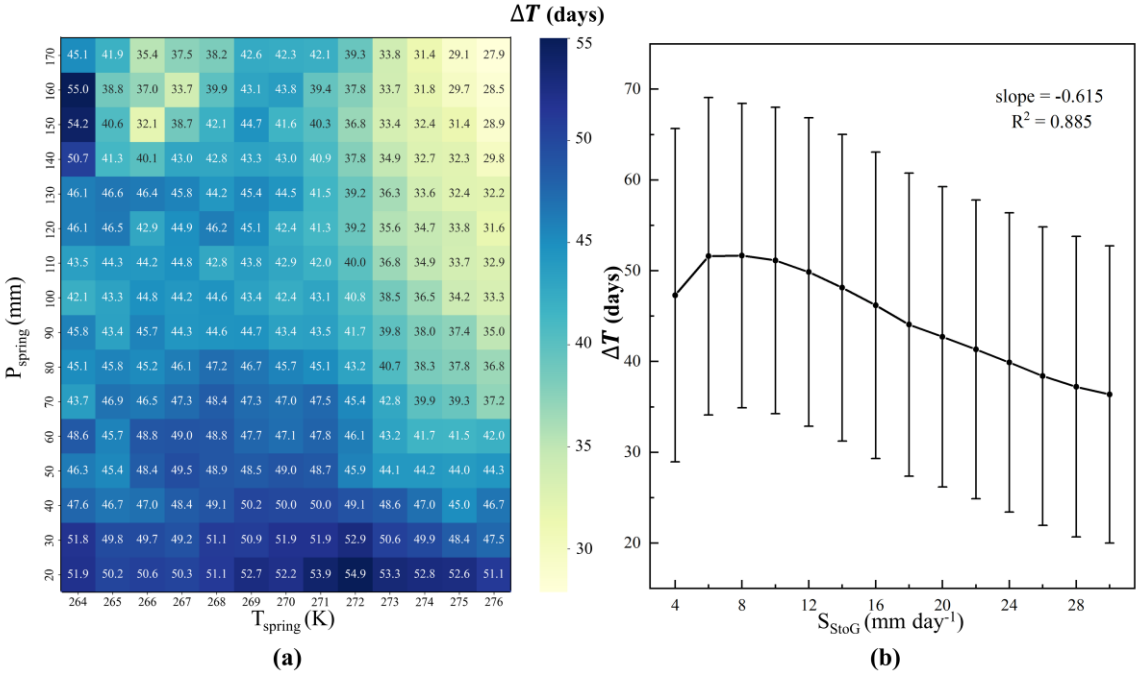

Figure 7: Variations in ΔT across regions with differing (a) spring mean temperature (T_{spring}), spring total rainfall (P_{spring}), and (b) daily snowmelt from T_{SOM} to T_{GU} (S_{StoG}). In (b), points represent the mean ΔT, while error bars denote one standard deviation. The slope and R^2 value reflect the coefficient and precision of the linear regression, respectively, with a significance level of 0.01.

To quantify the influence of environmental factors on ΔT across different regions, a partial correlation coefficient was calculated for each pixel (Fig. 8). Only pixels with valid ΔT over a 6-year period were included in the analysis.

At a significance level of 0.1, ΔT was significantly correlated with temperature in 15.7% of samples, with 59.4% showing a positive correlation. These positively correlated pixels were predominantly located in the southern part of the valid data, while negatively correlated pixels were concentrated in the northern regions. Regarding rainfall, 16.1% of the samples exhibited a significant correlation with ΔT, with 76.8% of these showing a negative correlation and 23.2% showing a positive one. Snowmelt demonstrated a significant relationship with ΔT in 25.8% of samples, with 86.1% showing a negative correlation, and the average correlation index was −0.46.

https://doi.org/10.5194/egusphere-2024-2885
Preprint. Discussion started: 16 October 2024

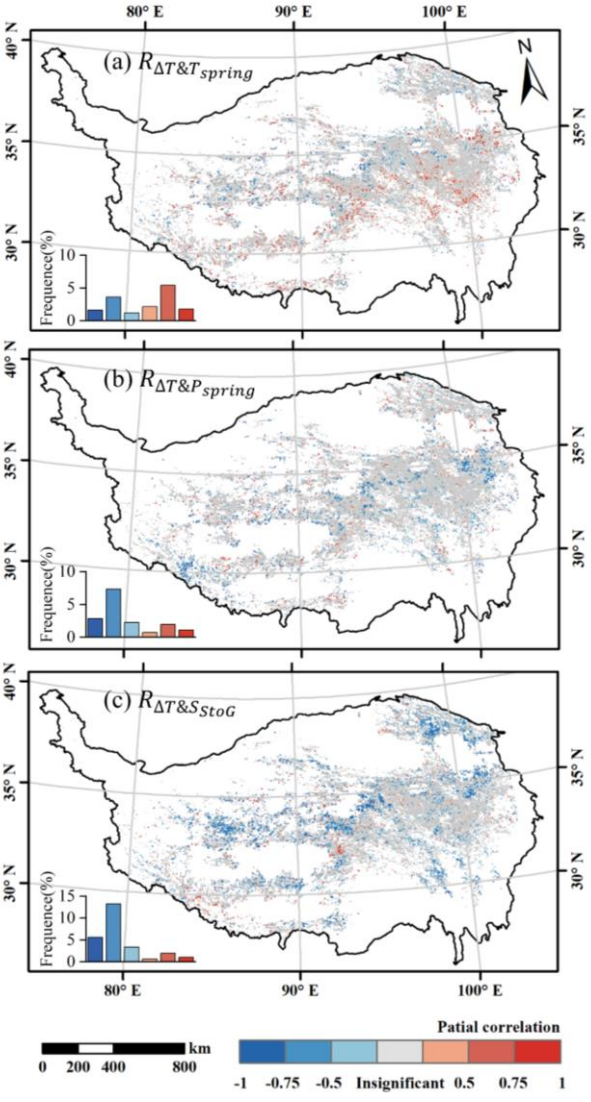

Figure 8: Spatial distribution of the partial correlation between ΔT and (a) spring mean temperature ($R_{\Delta T\&T_{spring}}$), (b) spring total rainfall ($R_{\Delta T\&P_{spring}}$), and (c) daily snowmelt from T_{SOM} to T_{GU} ($R_{\Delta T\&S_{StoG}}$).

A linear regression model was established to determine the dominant factor influencing ΔT at each pixel (Fig. 9). Among the significant samples (p<0.1), T_{spring}, P_{spring}, and S_{StoG} accounted for 40.9%, 11.1%, and 48.0% of the dominant factors, respectively. On the southeastern TP, T_{spring} primarily influences ΔT, whereas on the northwestern TP, S_{StoG} is more influential. This aligns with the distribution of vegetation types and geographical zones (Fig. 1). Consequently, the proportion of each dominant factor across different regions was assessed. In the arid zone, 74% of pixels were dominated by S_{StoG}, compared to 20% dominated by T_{spring}. As moisture increased, the dominant factor shifted from S_{StoG} to T_{spring}, with 65% of pixels in humid regions under temperature dominance and only 17% under S_{StoG}. Similarly, the proportion of

https://doi.org/10.5194/egusphere-2024-2885
Preprint. Discussion started: 16 October 2024

T_{spring}-dominant pixels increased from 22 to 59%, while S_{StoG}-dominant pixels decreased from 66 to 17% as vegetation became higher. Additionally, P_{spring}-dominant pixels consistently represented the lowest fractions (6–24%) across all regions.

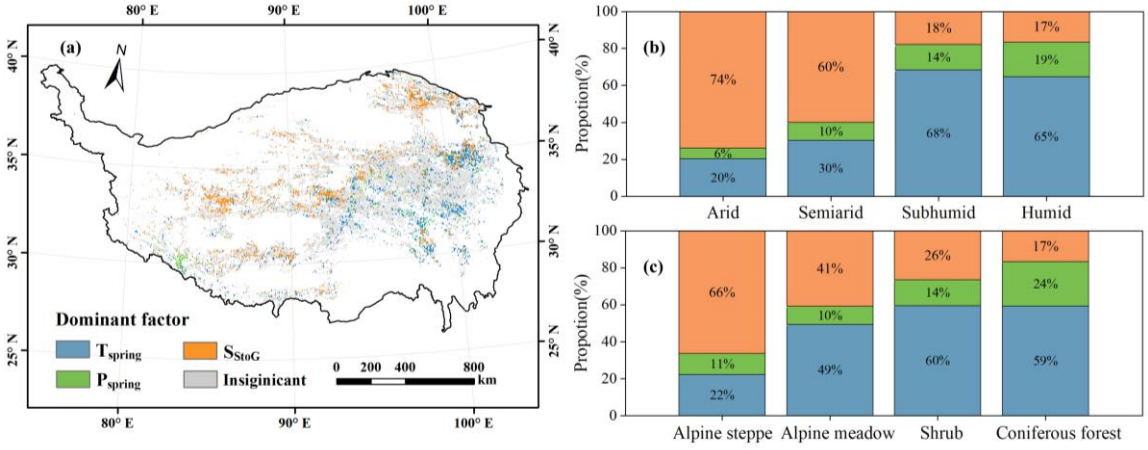

Figure 9: (a) Spatial distribution of dominant factor of ΔT and its proportion diagram among (b) different geographical zones and (c) different vegetation types.

4 Discussion

4.1 Quality evaluation of ΔT

ΔT is primarily determined by T_{SOM} and T_{GU}. Xu et al. (2022b) discussed the accuracy of T_{GU}, so this study focused on the identification quality of T_{SOM}.

T_{SOM} can currently be derived from optical or microwave remote sensing images. The Normalized Difference Snow Index (NDSI) is commonly used for snow identification in optical images. During periods of surface snow coverage, the NDSI tended to remain elevated and steady. After the start of snowmelt, the NDSI began to decrease. Consequently, T_{SOM} can be identified using the dynamic threshold method on the NDSI time-series curve (Potter, 2020; Zheng et al., 2022). However, NDSI mainly reflects snow presence rather than the snowmelt process, which initially reduces snow depth rather than snow cover extent (Panday et al., 2011).

Microwave bands, on the other hand, are more effective at tracking the internal state of snowpacks due to differences in the dielectric constant between water and snow (Ma et al., 2020). Melting snow leads to abrupt changes in brightness temperature or backscatter coefficient, facilitating T_{SOM} identification (Smith et al., 2017). Methods developed for this purpose include the band threshold method (Howell et al., 2012), the diurnal amplitude variation algorithm (DAV) (Semmens and Ramage, 2013), and the cross-polarized gradient ratio (Grippa et al., 2005). For instance, Xiong et al. (2017) identified T_{SOM} as the date when the differential average derivative of the Ku-band reached a maximum, providing the

https://doi.org/10.5194/egusphere-2024-2885
Preprint. Discussion started: 16 October 2024

snowmelt onset time for the High Mountain Asia (1979–2018) dataset (SOMHMA), available from the National Tibetan Plateau Scientific Data Center (https://data.tpdc.ac.cn/) with a spatial resolution of 0.25°.

Although this dataset captures snowmelt evolution, its spatial resolution is relatively low. T_{SOM} can also be indirectly identified from abrupt points in the snow depth/snow water equivalent time series (Fontrodona-Bach et al., 2023; Zheng et al., 2022). Our study used a snow depth dataset from section 2.2.2, which improved spatial resolution to 0.05° via downscaling while maintaining the benefits of microwave bands, making it more accurate than traditional microwave data with a 0.25° resolution.

Verifying T_{SOM} is challenging due to the lack of in situ data. Snowmelt patterns, influenced by external conditions and similar to temperature distributions, have been cross-validated with temperature records in previous studies (Drobot and Anderson, 2001; Panday et al., 2011; Zheng et al., 2020). Thus, following Grippa et al. (2005), we randomly selected four sample areas on the TP and calculated the correlation coefficient between average T_{SOM} and mean April temperature (Fig. 10). Our results showed stronger consistency with temperature trends compared to SOMHMA. The ΔT calculated by SOMHMA was relatively random and inconclusive (Fig. S1-S3), potentially due to mixed pixel issues from its limited resolution. Although our method offers improved accuracy, some errors in T_{SOM} persist due to original data uncertainty (RMSE = 0.61 cm) (Yan et al., 2022).

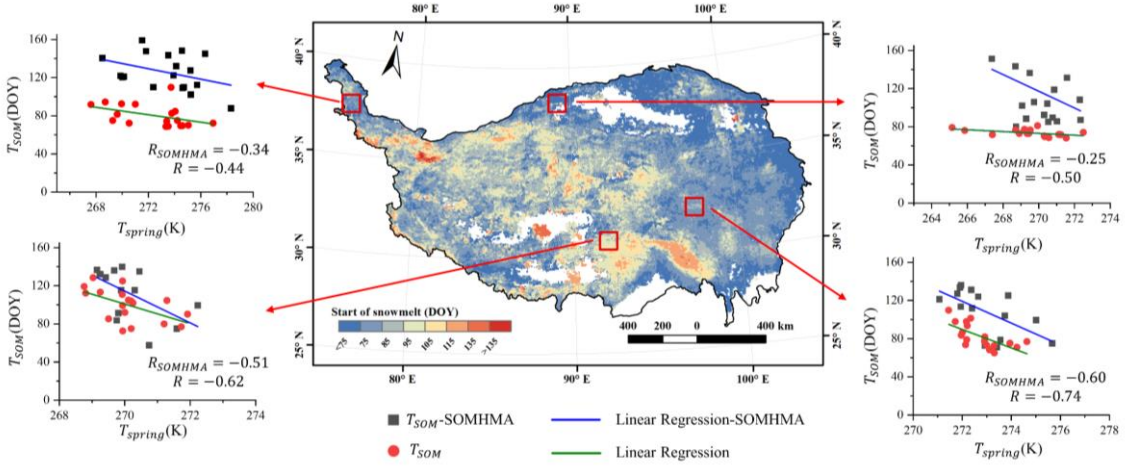

Figure 10: Relevance between the average T_{SOM} and mean April temperature in four sample areas.

4.2 Response of vegetation to snowmelt

In this study, the time difference between T_{GU} and T_{SOM} was defined as ΔT. This metric can have both positive and negative values, each with different implications. A positive ΔT indicates the time it takes for vegetation to respond to snowmelt. On the TP, ΔT was predominantly positive, with an average of 36.7 days. This suggests that vegetation response to snowmelt typically involves a delay of nearly one month. In contrast, response times are generally shorter in other regions. ΔT in the

https://doi.org/10.5194/egusphere-2024-2885
Preprint. Discussion started: 16 October 2024

high Arctic, Alaska, and Finland averaged 3 weeks (Cooper et al., 2011), 14.9 days (Zheng et al., 2022) and 5–13 days (Manninen et al., 2019), respectively.

The influence of S_{StoG} on response rate was notably widespread, with more S_{StoG} shortening the response time in one-fourth of the TP. It can be inferred that reductions in ice volume and increases in the rain-to-snow ratio due to global warming may influence vegetation sensitivity to snowmelt (Tomaszewska et al., 2020). Snowmelt primarily affects soil moisture and nutrients, thus stimulating vegetative response to T_{SOM}. Previous studies have emphasized the critical role of snowmelt in soil moisture. During early vegetation development, especially in alpine and cold regions, snow serves as an essential water source (Ernakovich et al., 2014; Li et al., 2020; Ma et al., 2024). This is evident in Fig. 9, where regions dominated by S_{StoG} were more extensive than those dominated by P_{spring}. Edwards et al. (2007) observed that nitrogen is leached from the snow layer during snowmelt and combines with nitrogen released from mineralization to form a pulse of inorganic nitrogen beneath the snow. This results in a peak in NO3− available post-snowmelt. As alpine vegetation typically prefers NO3− as a nitrogen source, snowmelt meets this need (Broadbent et al., 2021). Additionally, the insulating effect of snow on vegetation diminishes after melting (Rixen et al., 2022). For instance, Starr and Oberbauer (2003) measured solar radiation at different snow depths in the northern foothills of the Brooks Mountain Range, Alaska, finding that light levels were reduced by 20–40% under 10 cm of snow and declined up to 70% under 20 cm compared to bare ground. Thus, future remote sensing efforts should aim to quantify the snow's shielding effect to better understand vegetation response mechanisms.

The vegetation response to T_{SOM} is influenced not only by snowmelt but also by meteorological conditions. Temperature and precipitation, as primary factors of T_{GU}, significantly affect the response rate on the TP, accounting for 15.7% and 16.1% respectively (Fig. 8). Precipitation provides essential water for vegetation, enabling a swift return to growth post-snowmelt. Temperature, on the other hand, impacts the heat required for vegetation growth and accelerates snowmelt, thereby supplying water and nutrients (Liu et al., 2021). Higher temperature can thus enhance T_{GU} and shorten response time (Fig. 7a). However, elevated temperatures may also advance T_{SOM} (Mioduszewski et al., 2014; Mioduszewski et al., 2015). Due to the differential effects of temperature on T_{SOM} and T_{GU}, both positive and negative correlation between T_{spring} and ΔT were observed at local scales (Fig. 8a). Statistical analysis shows that positively correlated pixels are typically found in southern regions with an average T_{spring} of 271.19 K, while negatively correlated areas are in northern regions with an average T_{spring} of 269.84 K. In warmer regions with mean annual temperatures above freezing, spring temperature correlates negatively with T_{SOM} (−0.46) and T_{GU} (−0.07), indicating that temperature primarily influences snowmelt rather than vegetation growth, thus extending response times. Conversely, in colder regions, where spring temperatures correlate negatively with T_{SOM} (−0.28) and T_{GU} (−0.27), increased temperatures can reduce cold stress on vegetation. However, consistent sub-freezing temperatures do not significantly enhance T_{SOM}. In summary, the relationship between temperature and response time is modulated by the magnitudes of their respective influences at the local scale.

https://doi.org/10.5194/egusphere-2024-2885
Preprint. Discussion started: 16 October 2024

Furthermore, the primary factors controlling response time varied across regions but exhibited a clear regional distribution. Previous studies have indicated that in arid areas, T_{GU} is more sensitive to water availability, especially in the central and western TP, while T_{GU} shows a more significant negative correlation with temperature in the eastern TP, which experiences wetter springs (Piao et al., 2019; Shen et al., 2022). Despite differences in dependent variables, this conclusion remains consistent (Fig. 9b). In arid regions, where water is the main limiting factor, ΔT is predominantly controlled by snowmelt. In contrast, in humid regions where heat is the limiting factor, ΔT is mainly influenced by T_{spring}. When analyzing by vegetation type, higher vegetation (e.g., shrubs and forests), which is more exposed to the environment, is primarily influenced by temperature. Conversely, lower vegetation (e.g., alpine steppes and meadows), which is covered by snow, is more affected by snowmelt than by T_{spring} and P_{spring} (Fig. 9c). This finding is supported by Zheng et al. (2022), who observed that the growth rate of soil temperatures was higher in lower vegetation compared to higher vegetation. Our study, which compares these factors at the pixel scale, further substantiates this view and clarifies the spatial variations across the TP.

Specially, if ΔT is negative (i.e. T_{SOM} occurs later than T_{GU}), this situation is termed "false spring" (Chamberlain et al., 2019; Chamberlain et al., 2021; Peterson and Abatzoglou, 2014). During false springs, once plant growth begins, frost tolerance significantly decreases. Continued exposure to freezing conditions can damage vegetation tissues and reduce productivity, leading to both ecological and economic impacts (Chamberlain et al., 2019). Zhu et al. (2019b) used the SI-x model to simulate the probability of false spring in China from 1950 to 2005 and projected it until 2100, finding that the TP exhibited the highest probability in China. Thus, false spring warrants further investigation in the TP, even though it was not the primary focus of this study.

Although previous studies have established a strong positive correlation between T_{SOM} and T_{GU} (An et al., 2022; Wang et al., 2015; Wang et al., 2018b; Xu et al., 2022a), the specific time differences between them in the TP remain unclear. Our study advances this understanding by examining the heterogeneity and mechanisms of vegetation response to snowmelt and reinforces the notion that snowmelt primarily affects arid regions and areas with low vegetation cover.

5 Conclusion

In this study, we first identified the start of snowmelt (T_{SOM}) using snow depth products and integrated this with green-up date datasets to calculate ΔT from 2001 to 2018 on the TP. We further explored the effects of T_{spring}, P_{spring}, and S_{StoG} on ΔT through heatmaps, box plots, partial correlation analysis, and multiple linear regression. The results showed that (1) T_{SOM} ranged from DOY 70 to 100 across 80.1% of the TP, with an average of DOY 86.1. The average ΔT from 2001 to 2018 was 36.7 days, with ΔT being positive over 90% of the TP, which is longer compared to other regions due to snowpack characteristics. (2) Spatially, low ΔT was concentrated in the Hengduan Mountains, while high ΔT was observed in the Bayankara and Himalayas Mountains. Only 6.2% of the study area exhibited a significant temporal trend, attributed toa

https://doi.org/10.5194/egusphere-2024-2885
Preprint. Discussion started: 16 October 2024

warming hiatus. (3) At the significance level of 0.1, T_{spring}, P_{spring}, and S_{StoG} explained 15.7%, 16.1%, and 25.8% of ΔT variation, respectively, with negative correlation accounting for 40.6%, 76.8%, and 86.1%. (4) S_{StoG} was the dominant factor affecting ΔT for 74% and 66% of arid regions and areas with low vegetation respectively, while T_{spring} was predominant in humid and areas with high vegetation, affecting 65% and 59% of these regions. Our findings suggest that T_{SOM}, derived from downscaled snow depth dataset, provides more reliable information on the snow-melting process. Additionally, as a source of water and nitrogen, S_{StoG} significantly influences vegetation response to T_{SOM}. This study also confirms that vegetation in arid regions is more reliant on water than heat, and low-vegetation areas are more dependent on sub-snow habitat than external factors. These insights underscore the critical role of snowmelt in vegetation growth and enhance our understanding of vegetation responses to snowmelt. Future research should focus on the effects of snow cover and false springs.

Data availability

The data used in this study is all available on the request from the corresponding author.

Author Contribution

JN: Investigation, methodology, data curation, validation, visualization, wrting – original draft. JC: Conceptualization, methodology, formal analysis, writing - review & editing. YT: Methodology, formal analysis. JX: Methodology, resources. JX: Methodology, visualization. LD: Formal analysis. QG: Formal analysis. BY: Fomal analysis. JW: Fomal analysis. YH: Conceptualization, Project administration, Funding acquisition, Validation, Resources, Fomal analysis, Wrting – review & editing.

Competing interests

The authors declare that they have no conflict of interest.

Acknowledgments

This study was supported by the National Natural Science Foundation of China (No. 42071306). And we also thank the National Tibetan Plateau Data Center, the Climate Data Store, and the Science Data Bank for providing the required data.

https://doi.org/10.5194/egusphere-2024-2885
Preprint. Discussion started: 16 October 2024

References

An, S., Zhang, X., and Ren, S.: Spatial Difference between Temperature and Snowfall Driven Spring Phenology of Alpine Grassland Land Surface Based on Process-Based Modeling on the Qinghai-Tibet Plateau, Remote Sens., 14, https://doi.org/10.3390/rs14051273, 2022.

Bibi, S., Wang, L., Li, X. P., Zhou, J., Chen, D. L., and Yao, T. D.: Climatic and associated cryospheric, biospheric, and hydrological changes on the Tibetan Plateau: a review, Int. J. Climatol., 38, E1-E17, https://doi.org/10.1002/joc.5411, 2018.

Broadbent, A. A. D., Snell, H. S. K., Michas, A., Pritchard, W. J., Newbold, L., Cordero, I., Goodall, T., Schallhart, N., Kaufmann, R., Griffiths, R. I., Schloter, M., Bahn, M., and Bardgett, R. D.: Climate change alters temporal dynamics of alpine soil microbial functioning and biogeochemical cycling via earlier snowmelt, ISME J., 15, 2264-2275, https://doi.org/10.1038/s41396-021-00922-0, 2021.

Chamberlain, C. J., Cook, B. I., de Cortazar-Atauri, I. G., and Wolkovich, E. M.: Rethinking false spring risk, Global Change Biol., 25, 2209-2220, https://doi.org/10.1111/gcb.14642, 2019.

Chamberlain, C. J., Cook, B. I., Morales-Castilla, I., and Wolkovich, E. M.: Climate change reshapes the drivers of false spring risk across European trees, New Phytol., 229, 323-334, https://doi.org/10.1111/nph.16851, 2021.

Cooper, E. J., Dullinger, S., and Semenchuk, P.: Late snowmelt delays plant development and results in lower reproductive success in the High Arctic, Plant Sci., 180, 157-167, https://doi.org/10.1016/j.plantsci.2010.09.005, 2011.

Diao, C., Liu, Y., Zhao, L., Zhuo, G., and Zhang, Y. Q.: Regional-scale vegetation-climate interactions on the Qinghai-Tibet Plateau, Ecol. Inf., 65, https://doi.org/10.1016/j.ecoinf.2021.101413, 2021.

Dong, L., Zhou, H., Xu, J., Tang, Y., Teng, X., Ni, J., Yu, B., Wu, J., and Huang, Y.: BI or IB: Which Better Generates High Spatiotemporal Resolution NDSI by Fusing Sentinel-2A/B and MODIS Data?, IEEE J. Sel. Top. Appl. Earth Obs. Remote Sens., 17, 3314-3333, https://doi.org/10.1109/jstars.2023.3347202, 2024.

Drobot, S. D. and Anderson, M. R.: An improved method for determining snowmelt onset dates over Arctic sea ice using scanning multichannel microwave radiometer and Special Sensor Microwave/Imager data, J. Geophys. Res-atmos., 106, 24033-24049, https://doi.org/10.1029/2000jd000171, 2001.

Edwards, A. C., Scalenghe, R., and Freppaz, M.: Changes in the seasonal snow cover of alpine regions and its effect on soil processes: A review, Quat. Int., 162, 172-181, https://doi.org/10.1016/j.quaint.2006.10.027, 2007.

Ernakovich, J. G., Hopping, K. A., Berdanier, A. B., Simpson, R. T., Kachergis, E. J., Steltzer, H., and Wallenstein, M. D.: Predicted responses of arctic and alpine ecosystems to altered seasonality under climate change, Global Change Biol., 20, 3256-3269, https://doi.org/10.1111/gcb.12568, 2014.

Fontrodona-Bach, A., Schaefli, B., Woods, R., Teuling, A. J., and Larsen, J. R.: NH-SWE: Northern Hemisphere Snow Water Equivalent dataset based on in situ snow depth time series, Earth Syst. Sci. Data, 15, 2577-2599, https://doi.org/10.5194/essd-15-2577-2023, 2023.

Grippa, M., Mognard, N., and Le Toan, T.: Comparison between the interannual variability of snow parameters derived from SSM/I and the Ob river discharge, Remote Sens. Environ., 98, 35-44, https://doi.org/10.1016/j.rse.2005.06.001, 2005.

Guan, X., Guo, S., Huang, J., Shen, X., Fu, L., and Zhang, G.: Effect of seasonal snow on the start of growing season of typical vegetation in Northern Hemisphere, Geogr, Sustain., 3, 268-276, https://doi.org/10.1016/j.geosus.2022.09.001, 2022.

He, J., Yang, K., Tang, W. J., Lu, H., Qin, J., Chen, Y. Y., and Li, X.: The first high-resolution meteorological forcing dataset for land process studies over China, Sci. Data, 7, https://doi.org/10.1038/s41597-020-0369-y, 2020.

Howell, S. E. L., Assini, J., Young, K. L., Abnizova, A., and Derksen, C.: Snowmelt variability in Polar Bear Pass, Nunavut, Canada, from QuikSCAT: 2000-2009, Hydrol. Processes, 26, 3477-3488, https://doi.org/10.1002/hyp.8365, 2012.

Huang, K., Zu, J., Zhang, Y., Cong, N., Liu, Y., and Chen, N.: Impacts of snow cover duration on vegetation spring phenology over the Tibetan Plateau, J. Plant Ecol., 12, 583-592, https://doi.org/10.1093/jpe/rty051, 2019.

Lei, Y., Pan, J., Xiong, C., Jiang, L., and Shi, J.: Snow depth and snow cover over the Tibetan Plateau observed from space in against ERA5: matters of scale, Clim. Dyn., 60, 1523-1541, https://doi.org/10.1007/s00382-022-06376-0, 2023.

https://doi.org/10.5194/egusphere-2024-2885
Preprint. Discussion started: 16 October 2024

Li, Y., Li, T., Liu, D., Fu, Q., Hou, R., Ji, Y., and Cui, S.: Estimation of snow meltwater based on the energy and mass processes during the soil thawing period in seasonally frozen soil areas, Agric. For. Meteorol., 292, https://doi.org/10.1016/j.agrformet.2020.108138, 2020.

Li, Y. Z., Qin, X., Liu, Y. S., Jin, Z. Z., Liu, J., Wang, L. H., and Chen, J. Z.: Evaluation of Long-Term and High-Resolution Gridded Precipitation and Temperature Products in the Qilian Mountains, Qinghai-Tibet Plateau, Frontiers in Environmental Science, 10, https://doi.org/10.3389/fenvs.2022.906821, 2022.

Liu, H., Xiao, P., Zhang, X., Chen, S., Wang, Y., and Wang, W.: Winter snow cover influences growing-season vegetation productivity non-uniformly in the Northern Hemisphere, Commun. Earth Environ., 4, https://doi.org/10.1038/s43247-023-01167-9, 2023.

Liu, X. G., Chen, Y. N., Li, Z., Li, Y. P., Zhang, Q. F., and Zan, M.: Driving Forces of the Changes in Vegetation Phenology in the Qinghai-Tibet Plateau, Remote Sens., 13, https://doi.org/10.3390/rs13234952, 2021.

Ma, W., Hu, J., Zhang, B., Guo, J., Zhang, X., and Wang, Z.: Later-melting rather than thickening of snowpack enhance the productivity and alter the community composition of temperate grassland, Sci. Total Environ., 923, https://doi.org/10.1016/j.scitotenv.2024.171440, 2024.

Ma, W., Xiao, P., Zhang, X., Song, Y., Ma, T., and Ye, L.: Retrieving snow wetness based on surface and volume scattering simulation, ISPRS J. Photogramm. Remote Sens., 169, 17-28, https://doi.org/10.1016/j.isprsjprs.2020.08.021, 2020.

Manninen, T., Aalto, T., Markkanen, T., Peltoniemi, M., Bottcher, K., Metsamaki, S., Anttila, K., Pirinen, P., Leppanen, A., and Arslan, A. N.: Monitoring changes in forestry and seasonal snow using surface albedo during 1982-2016 as an indicator, Biogeosciences, 16, 223-240, https://doi.org/10.5194/bg-16-223-2019, 2019.

Mioduszewski, J. R., Rennermalm, A. K., Robinson, D. A., and Mote, T. L.: Attribution of snowmelt onset in Northern Canada, J. Geophys. Res-atmos., 119, 9638-9653, https://doi.org/10.1002/2013jd021024, 2014.

Mioduszewski, J. R., Rennermalm, A. K., Robinson, D. A., and Wang, L.: Controls on Spatial and Temporal Variability in Northern Hemisphere Terrestrial Snow Melt Timing, 1979-2012, J. Clim., 28, 2136-2153, https://doi.org/10.1175/jcli-d-14-00558.1, 2015.

Panday, P. K., Frey, K. E., and Ghimire, B.: Detection of the timing and duration of snowmelt in the Hindu Kush-Himalaya using QuikSCAT, 2000-2008, Environ. Res. Lett., 6, https://doi.org/10.1088/1748-9326/6/2/024007, 2011.

Peng, S., Piao, S., Ciais, P., Fang, J., and Wang, X.: Change in winter snow depth and its impacts on vegetation in China, Global Change Biol., 16, 3004-3013, https://doi.org/10.1111/j.1365-2486.2010.02210.x, 2010.

Peterson, A. G. and Abatzoglou, J. T.: Observed changes in false springs over the contiguous United States, Geophys. Res. Lett., 41, 2156-2162, https://doi.org/10.1002/2014gl059266, 2014.

Piao, S., Liu, Q., Chen, A., Janssens, I. A., Fu, Y., Dai, J., Liu, L., Lian, X., Shen, M., and Zhu, X.: Plant phenology and global climate change: Current progresses and challenges, Global Change Biol., 25, 1922-1940, https://doi.org/10.1111/gcb.14619, 2019.

Potter, C.: Snowmelt timing impacts on growing season phenology in the northern range of Yellowstone National Park estimated from MODIS satellite data, Landscape Ecol., 35, 373-388, https://doi.org/10.1007/s10980-019-00951-3, 2020.

Ren, Y., Zhang, L., Yang, K., Li, Z., Yin, R., Tan, B., Wang, L., Liu, Y., Li, H., You, C., Liu, S., Xu, Z., and Kardol, P.: Short-term effects of snow cover manipulation on soil bacterial diversity and community composition, Sci. Total Environ., 741, https://doi.org/10.1016/j.scitotenv.2020.140454, 2020.

Rixen, C., Høye, T. T., Macek, P., Aerts, R., Alatalo, J. M., Anderson, J. T., Arnold, P. A., Barrio, I. C., Bjerke, J. W., Björkman, M. P., Blok, D., Blume-Werry, G., Boike, J., Bokhorst, S., Carbognani, M., Christiansen, C. T., Convey, P., Cooper, E. J., Cornelissen, J. H. C., Coulson, S. J., Dorrepaal, E., Elberling, B., Elmendorf, S. C., Elphinstone, C., Forte, T. a. G. W., Frei, E. R., Geange, S. R., Gehrmann, F., Gibson, C., Grogan, P., Halbritter, A. H., Harte, J., Henry, G. H. R., Inouye, D. W., Irwin, R. E., Jespersen, G., Jónsdóttir, I. S., Jung, J. Y., Klinges, D. H., Kudo, G., Lämsä, J., Lee, H., Lembrechts, J. J., Lett, S., Lynn, J. S., Mann, H. M. R., Mastepanov, M., Morse, J., Myers-Smith, I. H., Olofsson, J., Paavola, R., Petraglia, A., Phoenix, G. K., Semenchuk, P., Siewert, M. B., Slatyer, R., Spasojevic, M. J., Suding, K., Sullivan, P., Thompson, K. L., Väisänen, M., Vandvik, V., Venn, S., Walz, J., Way, R., Welker, J. M., Wipf, S., and Zong, S.: Winters are changing: snow effects on Arctic and alpine tundra ecosystems, Arct. Sci., 8, 572 - 608, 2022.

https://doi.org/10.5194/egusphere-2024-2885
Preprint. Discussion started: 16 October 2024

Semmens, K. A. and Ramage, J. M.: Recent changes in spring snowmelt timing in the Yukon River basin detected by passive microwave satellite data, Cryosphere, 7, 905-916, https://doi.org/10.5194/tc-7-905-2013, 2013.

Shen, M., Wang, S., Jiang, N., Sun, J., Cao, R., Ling, X., Fang, B., Zhang, L., Zhang, L., Xu, X., Lv, W., Li, B., Sun, Q., Meng, F., Jiang, Y., Dorji, T., Fu, Y., Iler, A., Vitasse, Y., Steltzer, H., Ji, Z., Zhao, W., Piao, S., and Fu, B.: Plant phenology changes and drivers on the Qinghai-Tibetan Plateau, Nat. Rev. Earth Environ., 3, 633-651, https://doi.org/10.1038/s43017-022-00317-5, 2022.

Shen, M. G., Zhang, G. X., Cong, N., Wang, S. P., Kong, W. D., and Piao, S. L.: Increasing altitudinal gradient of spring vegetation phenology during the last decade on the Qinghai-Tibetan Plateau, Agric. For. Meteorol., 189, 71-80, https://doi.org/10.1016/j.agrformet.2014.01.003, 2014.

Shen, M. G., Piao, S. L., Dorji, T., Liu, Q., Cong, N., Chen, X. Q., An, S., Wang, S. P., Wang, T., and Zhang, G. X.: Plant phenological responses to climate change on the Tibetan Plateau: research status and challenges, Natl. Sci. Rev., 2, 454-467, https://doi.org/10.1093/nsr/nwv058, 2015.

Smith, T., Bookhagen, B., and Rheinwalt, A.: Spatiotemporal patterns of High Mountain Asia's snowmelt season identified with an automated snowmelt detection algorithm, 1987-2016, Cryosphere, 11, 2329-2343, https://doi.org/10.5194/tc-11-2329-2017, 2017.

Stanislaw, K., Pawel, C., Danuta, K., and Robert, P.: Variability and changes of the height and duration of snow cover on the Gasienicowa Glade (Tatras), Int. J. Climatol., 43, 7018-7031, https://doi.org/10.1002/joc.8249, 2023.

Starr, G. and Oberbauer, S. F.: Photosynthesis of arctic evergreens under snow: Implications for tundra ecosystem carbon balance, Ecology, 84, 1415-1420, https://doi.org/10.1890/02-3154, 2003.

Tomaszewska, M. A., Nguyen, L. H., and Henebry, G. M.: Land surface phenology in the highland pastures of montane Central Asia: Interactions with snow cover seasonality and terrain characteristics, Remote Sens. Environ., 240, 111675, https://doi.org/https://doi.org/10.1016/j.rse.2020.111675, 2020.

Wang, K., Zhang, L., Qiu, Y., Ji, L., Tian, F., Wang, C., and Wang, Z.: Snow effects on alpine vegetation in the Qinghai-Tibetan Plateau, Int. J. Digital Earth, 8, 56-73, https://doi.org/10.1080/17538947.2013.848946, 2015.

Wang, X., Wu, C., Peng, D., Gonsamo, A., and Liu, Z.: Snow cover phenology affects alpine vegetation growth dynamics on the Tibetan Plateau: Satellite observed evidence, impacts of different biomes, and climate drivers, Agric. For. Meteorol., 256, 61-74, https://doi.org/10.1016/j.agrformet.2018.03.004, 2018a.

Wang, X., Xiao, J., Li, X., Cheng, G., Ma, M., Zhu, G., Arain, M. A., Black, T. A., and Jassal, R. S.: No trends in spring and autumn phenology during the global warming hiatus, Nat. Commun., 10, https://doi.org/10.1038/s41467-019-10235-8, 2019.

Wang, X. Y., Wang, T., Guo, H., Liu, D., Zhao, Y. T., Zhang, T. T., Liu, Q., and Piao, S. L.: Disentangling the mechanisms behind winter snow impact on vegetation activity in northern ecosystems, Global Change Biol., 24, 1651-1662, https://doi.org/10.1111/gcb.13930, 2018b.

Wu, Y., Xiao, P., Zhang, X., Liu, H., Dong, Y., and Feng, L.: Effects of Snow Cover on Spring Vegetation Phenology Vary With Temperature Gradient Across the Pan-Arctic, J. Geophys, Res. :Biogeosci., 128, https://doi.org/10.1029/2022jg007183, 2023.

Xiong, C., Shi, J., Cui, Y., and Peng, B.: Snowmelt Pattern Over High-Mountain Asia Detected From Active and Passive Microwave Remote Sensing, IEEE Geosci. Remote Sens. Lett., 14, 1096-1100, https://doi.org/10.1109/lgrs.2017.2698448, 2017.

Xiong, T., Zhang, H., Zhao, J., Zhang, Z., Guo, X., Zhu, Z., and Shan, Y.: Diverse Responses of Vegetation Dynamics to Snow Cover Phenology over the Boreal Region, Forests, 10, https://doi.org/10.3390/f10050376, 2019.

Xu, J., Tang, Y., Dong, L., Wang, S., Yu, B., Wu, J., Zheng, Z., and Huang, Y.: Temperature-dominated spatiotemporal variability in snow phenology on the Tibetan Plateau from 2002 to 2022, Cryosphere, 18, 1817-1834, https://doi.org/10.5194/tc-18-1817-2024, 2024.

Xu, J. Y., Tang, Y., Xu, J. H., Shu, S., Yu, B. L., Wu, J. P., and Huang, Y.: Impact of Snow Cover Phenology on the Vegetation Green-Up Date on the Tibetan Plateau, Remote Sens., 14, https://doi.org/10.3390/rs14163909, 2022a.

Xu, J. Y., Tang, Y., Xu, J. H., Chen, J., Bai, K. X., Shu, S., Yu, B. L., Wu, J. P., and Huang, Y.: Evaluation of Vegetation Indexes and Green-Up Date Extraction Methods on the Tibetan Plateau, Remote Sens., 14, https://doi.org/10.3390/rs14133160, 2022b.

https://doi.org/10.5194/egusphere-2024-2885
Preprint. Discussion started: 16 October 2024

Yan, D., Ma, N., and Zhang, Y.: Development of a fine-resolution snow depth product based on the snow cover probability for the Tibetan Plateau: Validation and spatial-temporal analyses, J. Hydrol., 604, https://doi.org/10.1016/j.jhydrol.2021.127027, 2022.

Yang, M. X., Wang, X. J., Pang, G. J., Wang, G. N., and Liu, Z. C.: The Tibetan Plateau cryosphere: Observations and model simulations for current status and recent changes, Earth Sci. Rev., 190, 353-369, https://doi.org/10.1016/j.earscirev.2018.12.018, 2019.

Yang, T., Li, Q., Zou, Q., Hamdi, R., Cui, F. Q., and Li, L. H.: Impact of Snowpack on the Land Surface Phenology in the Tianshan Mountains, Central Asia, Remote Sens., 14, https://doi.org/10.3390/rs14143462, 2022.

Zhang, J., Chen, S. Z., Wu, Z. F., and Fu, Y. H.: Review of vegetation phenology trends in China in a changing climate, Prog. Phys. Geogr.: Earth Environ., 46, 829-845, https://doi.org/10.1177/03091333221114737, 2022a.

Zhang, Q., Kong, D. D., Shi, P. J., Singh, V. P., and Sun, P.: Vegetation phenology on the Qinghai-Tibetan Plateau and its response to climate change (1982-2013), Agric. For. Meteorol., 248, 408-417, https://doi.org/10.1016/j.agrformet.2017.10.026, 2018a.

Zhang, Q., Yuan, R. Y., Singh, V. P., Xu, C. Y., Fan, K. K., Shen, Z. X., Wang, G., and Zhao, J. Q.: Dynamic vulnerability of ecological systems to climate changes across the Qinghai-Tibet Plateau, China, Ecol. Indic., 134, https://doi.org/10.1016/j.ecolind.2021.108483, 2022b.

Zhang, X. Y., Friedl, M. A., Schaaf, C. B., Strahler, A. H., Hodges, J. C. F., Gao, F., Reed, B. C., and Huete, A.: Monitoring vegetation phenology using MODIS, Remote Sens. Environ., 84, 471-475, https://doi.org/10.1016/s0034-4257(02)00135-9, 2003.

Zhang, Y., Sherstiukov, A. B., Qian, B., Kokelj, S. V., and Lantz, T. C.: Impacts of snow on soil temperature observed across the circumpolar north, Environ. Res. Lett., 13, https://doi.org/10.1088/1748-9326/aab1e7, 2018b.

Zhao, D. S., Wu, S. H., Yin, Y. H., and Yin, Z. Y.: Vegetation distribution on Tibetan Plateau under climate change scenario, Reg. Environ. Change, 11, 905-915, https://doi.org/10.1007/s10113-011-0228-7, 2011.

Zheng, J., Jia, G., and Xu, X.: Earlier snowmelt predominates advanced spring vegetation greenup in Alaska, Agric. For. Meteorol., 315, https://doi.org/10.1016/j.agrformet.2022.108828, 2022.

Zheng, L., Zhou, C., Zhang, T., Liang, Q., and Wang, K.: Recent changes in pan-Antarctic region surface snowmelt detected by AMSR-E and AMSR2, Cryosphere, 14, 3811-3827, https://doi.org/10.5194/tc-14-3811-2020, 2020.

Zhu, L., Ives, A. R., Zhang, C., Guo, Y., and Radeloff, V. C.: Climate change causes functionally colder winters for snow cover-dependent organisms, Nat. Clim. Change, 9, 886-+, https://doi.org/10.1038/s41558-019-0588-4, 2019a.

Zhu, L. K., Meng, J. J., Li, F., and You, N. S.: Predicting the patterns of change in spring onset and false springs in China during the twenty-first century, Int. J. Biometeorol., 63, 591-606, https://doi.org/10.1007/s00484-017-1456-4, 2019b.

Zou, Y. F., Sun, P., Ma, Z. C., Lv, Y. F., and Zhang, Q.: Snow Cover in the Three Stable Snow Cover Areas of China and Spatio-Temporal Patterns of the Future, Remote Sens., 14, https://doi.org/10.3390/rs14133098, 2022.